A new look to 275 to 400 GHz band: Channel model and performance evaluation

Evangelos N. Papasotiriou*, Joonas Kokkoniemi†, Alexandros-Apostolos A. Boulogeorgos*
Janne Lehtomäki†, Angeliki Alexiou*, and Markku Juntti†
*Department of Digital Systems, University of Piraeus, Piraeus 18534, Greece.
E-mails: al.boulogeorgos@ieee.org, {vangpapasot, alexiou}@unipi.gr
†Centre for Wireless Communications (CWC), University of Oulu, 90014 Oulu, Finland.
E-mail: joonas.kokkoniemi, janne.lehtomaki, markku.juntti@oulu.fi

***Abstract*—In this paper, we present a novel two-path channel model for wireless terahertz (THz) systems operating in the range of 275 to 400 GHz, which accommodates both the channel particularities and the transceivers parameters. The channel particularities include the frequency selectivity, path-loss, as well as the atmospheric conditions, namely temperature, relative humidity and pressure, while the transceiver parameters, which are taken into account, are the antenna gains as well as the power of the transmitted signal. Finally, we evaluated the THz system performance in terms of average signal to noise ratio and ergodic capacity.**

I. Introduction

Wireless data traffic has drastically increased accompanied by an increasing demand for higher data rate transmissions [1], [2]. In particular and according to the Edholm's law of bandwidth, wireless data rates have been doubled every 18 months over the last three decades and are quickly approaching the capacity of wired communication systems. Towards this end, terahertz (THz) band wireless communications have been recognized as an attractive canditate for providing an order of magnitude capacity improvements [3]–[7].

Despite the fact that wireless THz systems can gain from an extreme boost in bandwidth they suffer severe path attenuations, which significantly constraints the range [6], [8]. In order to countermeasure this issue, a great amount of effort has been put on modeling the channel particularities in the THz band (see for example [9]–[13] and references therein). In more detail, in [9], the authors introduced a path-loss model for nano-sensor networks operating in the THz band for plant foliage applications, whereas, in [10], a channel model for intra-body nano-scale communications was presented. Likewise, in [12], a model, which quantifies the total absorption loss assuming that air, natural gas and/or water are the components of the propagation medium, was provided. Finally, in [13], a multi-ray THz propagation model was presented. All the published work agrees on the fact that the wireless THz channel has a strong dependence on both the molecular composition of the medium and the transmission distance.

The results of the above presented models were capitalized in several works, including [14]–[17], where performance metrics for the THz link effectiveness were presented. In particular, in [14] the capacity of electromagnetic THz nano-sensor networks was analyzed, while, in [15] the authors expanded this analysis and revealed that there exist a relation between the transparency windows and the transmission distance. Likewise, in [16] the fundamental properties of THz-waves were investigated and the maximum achievable data rates for fixed wireless THz-links were evaluated, whereas in [18] the authors analyzed the channel behavior in order to design reconfigurable multiple input multiple output (MIMO) systems. In all of the mentioned works, the channel models employ the high-resolution transmission molecular absorption (HITRAN) database in order to take into account the impact of the molecular absorption loss. However, this leads to a difficulty in evaluating and quantifying the performance of wireless THz systems, as well as to provide the appropriate design guidelines and tools. On the other hand, in [17], the authors used a simplified path loss model and evaluated the THz link performance. However, in this work only the line of sight (LoS) component was taken into account.

Motivated by the above, in this paper, we provide a novel two-path channel model for wireless THz systems that operate in the range of 275 to 400 GHz, which accommodates the impact of both the LoS and the reflected components. Moreover, we provide analytical expressions for the evaluation of the link's ergodic capacity. In particular, by presenting the simplified path gain model, which takes into account the reflection losses, we are able to evaluate the average SNR, and capacity for THz links in the range of $275 - 400$ GHz. Our results reveal the performance dependency of the wireless THz system on the transmission environment, the communication bandwidth, the distance between the transmitter (TX) and the receiver (RX), and the gain of the TX and RX antennas. As a result, they can play a significant role as design tools for THz wireless systems.

II. System and Channel Model

In this section, we present the system model. In more detail, in Section II-A, the signal model and the assumption of our analysis are provided, whereas in Section II-B, the channel model for the 275–400 band is presented.

A. Signal Model

We assume that the transmitted signal s is conveyed over a wireless THz channel h, with an additive white Gaussian noise (AWGN) n. The baseband equivalent received signal can be obtained as

$$r = h * s + n, \tag{1}$$

where the operator $*$ stands for the convolution, h denotes the channel coefficient, and n represents the zero-mean circularly symmetric complex AWGN with single-sided power spectrum densities (PSD) equals N_0. Moreover, it is assumed that in order to countermeasure the severe THz channel path-losses as well as to constrain the power consumption of the transceivers, both the TX and RX employ analog beamforming.

According to (1) and based on the Parseval's theorem, the received signal power P_r, of a transmitted signal with single-sided power spectral density (PSD) $S(f)$, at the RX and bandwidth B can be evaluated as in [11], [19]

$$P_r = \int_B S(f)|H(f,d)|^2 \mathrm{df}, \tag{2}$$

where f stands for the frequency, d is the distance between the TX and RX, and

$$H(f,d) = H_c(f,d)H_r(f), \tag{3}$$

where $H_c(f,d)$ and $H_r(f)$ represent the THz band channel and the RX frequency responses respectively. By assuming an ideal low-pass filter with bandwidth B, (2) can be simplified as

$$P_r^i = \int_B S(f)|H_c(f,d)|^2 \mathrm{df}, \tag{4}$$

or equivalently

$$P_r^i = \int_B S(f)L(f,d) \mathrm{df}, \tag{5}$$

where $L(f,d)$ denotes the total path gain. Note that different distributions can be adopted for the transmitted signal's PSD. However, since the main scope of this paper is to present a simplified two-path channel model for wireless THz communications, to reveal the two-path THz channel particularities, we assume the simplest transmitted signal PSD, i.e.,

$$S_f(f) = \begin{cases} S_0, & \text{for } f \in B, \\ 0, & \text{elsewhere} \end{cases}, \tag{6}$$

where S_0 is constant. This is in line with several published papers in the technical literature, as well as with the fact, that there might be limitations in the affordable complexity of THz transceivers [20].

B. Channel Model

In this paper, we consider a two-path channel, which consists of one LOS and one reflected component. In this case the total path gain of the additive multipath components can be expressed as

$$\begin{aligned} L(f,d) = \Bigg| & L_f(f,d)L_a(f,d)\exp\left(-j\frac{2\pi f d}{c}\right) + \\ & L_r(\alpha)L_f(f,r_1+r_2)L_a(f,r_1+r_2) \\ & \times \exp\left(-j\frac{2\pi f(r_1+r_2)}{c} - j\pi\right)\Bigg|^2, \end{aligned} \tag{7}$$

where $L_f(f,d)$ and $L_a(f,d)$ are the free space and molecular absorption path gains, respectively. Moreover, $L_r(\alpha)$ denotes the reflection loss at angle α. The parameters f, d, r_1, and r_2 respectively stand for the frequency, the distance between the TX and RX, the distance from TX to the reflecting point, and the distance from the reflecting point to the RX.

According to the Friis transmission formula, the free space path gain can be obtained as

$$\mathrm{L_f} = \frac{c\sqrt{G_\mathrm{t}(\Theta_i)G_\mathrm{r}(\Theta_r)}}{4\pi df}, \tag{8}$$

where $G_\mathrm{t}(\Theta_i)$ and $G_\mathrm{r}(\Theta_r)$ represent the antenna orientation dependent TX and RX antenna gains respectively. Likewise, c stands for the speed of light. Finally, by assuming that the TX and RX are aligned, we get that $G_\mathrm{t}(\Theta_i) = G_t$ and $G_\mathrm{r}(\Theta_r) = G_r$.

On the other hand, the molecular absorption loss in the millimeter and THz frequency bands can be modeled by Beer-Lambert's law [14]

$$L_a(f,d) = \sqrt{\tau(f,d)} = \sqrt{\frac{P_\mathrm{r}(f,d)}{P_\mathrm{t}(f)}} = e^{-\frac{1}{2}\kappa_\mathrm{a}(f)d}, \tag{9}$$

where $\tau(f,d)$ denotes the transmittance, while $P_\mathrm{t}(f)$ represents the transmit power, and $\kappa_\mathrm{a}(f)$ stands for the absorption coefficient describing the relative absorbing area of the molecules in the medium per unit volume. It is worth noting that the main cause of absorption loss in the millimeter and THz frequencies is the water vapor, which causes deterministic frequency-dependent loss to the transmitted signal. Other molecules such as oxygen, also cause some level of attenuation to the signals, but the water vapor effect dominates the overall molecular absorption loss above 200 GHz frequencies.

We utilize a simplified model for the molecular absorption loss in 275–400 GHz band as shown in [21], [22]. The absorption coefficient can be evaluated by

$$\kappa_\mathrm{a}(f) = y_1(f,\mu) + y_2(f,\mu) + g(f), \tag{10}$$

where the parameters $y_1(f,\mu)$, and $y_2(f,\mu)$, and $g(f)$

of (18) can be expressed as

$$y_1(f,\mu) = \frac{A(\mu)}{B(\mu) + \left(\frac{f}{100c} - c_1\right)^2}, \tag{11}$$

$$y_2(f,\mu) = \frac{C(\mu)}{D(\mu) + \left(\frac{f}{100c} - c_2\right)^2}, \tag{12}$$

and

$$g(f) = p_1 f^3 + p_2 f^2 + p_3 f + p_4, \tag{13}$$

where $c_1 = 10.835$ cm^{-1}, $c_2 = 12.664$ cm^{-1}, $p_1 = 5.54 \times 10^{-37}$ Hz^{-3}, $p_2 = -3.94 \times 10^{-25}$ Hz^{-2}, $p_3 = 9.06 \times 10^{-14}$ Hz^{-1}, $p_4 = -6.36 \times 10^{-3}$,

$$A(\mu) = 0.2205\mu(0.1303\mu + 0.0294), \tag{14}$$

$$B(\mu) = (0.4093\mu + 0.0925)^2, \tag{15}$$

$$C(\mu) = 2.014\mu(0.1702\mu + 0.0303), \tag{16}$$

$$D(\mu) = (0.537\mu + 0.0956)^2. \tag{17}$$

and μ is the volume mixing ratio of the water vapor. This model was shown to have high accuracy for up to 1 km links in the standard atmospheric conditions, i.e., temperature of 296 °K and pressure of 101325 Pa [21]. Moreover, since the impact of the temperature and pressure can be modeled through the water vapor mixing ratio μ (18) can describe the THz link molecular absorption path loss beyond the standard atmospheric conditions. Finally, note that the parameters c_1, c_2, p_1, p_2, p_3, and p_4 can be considered relatively independent of the atmospheric conditions [21][1].

By combining (9) and (10), the molecular absorption gain can be given as

$$\mathrm{L_a}(f,d,\mu) = \exp\left(-\frac{d}{2}(y_1(f,\mu) + y_2(f,\mu) + g(f))\right), \tag{18}$$

$$\mu = \frac{\phi}{100}\frac{p_w(T,p)}{p}, \tag{19}$$

where ϕ and p are the relative humidity and the pressure respectively, $p_w(T,p)$ is the saturated water vapor partial pressure in temperature T and can be calculated according to Buck equation [23].

The reflection loss is evaluated according to the Fresnel's expressions [24]

$$R_s(\alpha) = \left|\frac{n_1\cos(\alpha) - n_2\sqrt{1 - (\frac{n_1}{n_2}\sin(\alpha))^2}}{n_1\cos(\alpha) + n_2\sqrt{1 - (\frac{n_1}{n_2}\sin(\alpha))^2}}\right|^2, \tag{20}$$

$$R_p(\alpha) = \left|\frac{n_1\sqrt{1 - (\frac{n_1}{n_2}\sin(\alpha))^2} - n_2\cos(\alpha)}{n_1\sqrt{1 - (\frac{n_1}{n_2}\sin(\alpha))^2} + n_2\cos(\alpha)}\right|^2, \tag{21}$$

[1]More details on the molecular absorption model, which is described by (18), and its derivations can be found in [21].

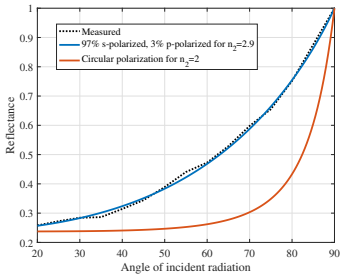

Fig. 1: Reflectance of the laminated particle board: measured, fitted refractive index, and equivalent reflectance for a circular polarization.

$$L_r(\alpha) = \sqrt{\frac{1}{2}(R_s(\alpha) + R_p(\alpha))}, \tag{22}$$

where $R_s(\alpha)$ and $R_p(\alpha)$ are the reflectances of the perpendicular and parallel components, respectively, of the electromagnetic wave to the reflecting surface, n_1 and n_2 are the refractive indices of air and reflecting material, respectively, and $L_r(\alpha)$ is the reflectance assuming circular polarization. We assume that the reflecting surface is a laminated particle board. We characterized this material using real-life measurements and assuming the refractive index of air (n_1) to be one. We fitted the measurement data to the Fresnel equations and found that the refractive index of laminated particle board equals $n_2 = 2.9$ at 300 GHz frequency. The measurement device strongly polarizes the radiation. As illustrated in Fig. 1, by modeling the reflections by refractive indices, we can give equivalent results for circular polarization. Furthermore, we assume that the phase is flipped 180 degrees as a consequence of the reflection.

The total channel gain can be evaluated by combining (7), (8), (18), and (22). Thus, the total path gain is dependent on the frequency, distance, and the angle of the reflection.

III. Performance Evaluation

In order to quantify the potential of the THz band for wireless communications, in this section we present fundamental link quality performance metrics namely, SNR and capacity.

A. SNR

According to (1), the SNR can be expressed as

$$\gamma(f,d,B,\mu) = \frac{P_r^i}{BN_0}. \tag{23}$$

By substituting (5) into (23), SNR can be equivalently rewritten as

$$\gamma(f,d,B,\mu) = \frac{S_0}{BN_0}\int_B L(f,d)\mathrm{d}f, \tag{24}$$

where $L(f,d)$ was found in (7).

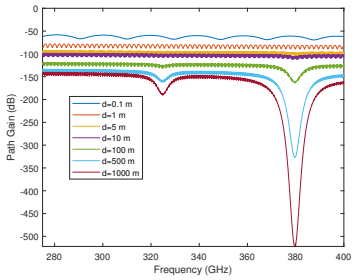

Fig. 2: Path gain as a function of the operation frequency for different transmission distances, assuming $G_t = G_r = 1$ and standard atmospheric conditions.

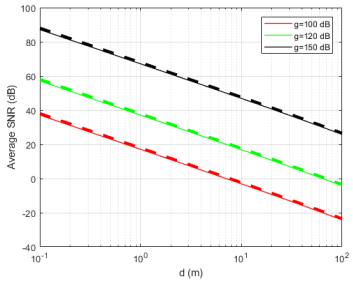

Fig. 3: SNR versus the distance for different values of g for $\alpha = \pi/3$ (dashed lines) and without reflection (continuous lines), assuming flat transmission signal PSD, $B = 125$ GHz, and standard atmospheric conditions.

B. Capacity

Since the THz channel is highly frequency dependent and under the common assumption that the transmitted signal and the total noise are jointly Gaussian the capacity C of the transparency window in the THz band can be estimated by employing the classic Shannon result for coherent reception as [15]

$$C = \int_B \log_2 \left(1 + \tilde{\gamma}(f, d)\right) \mathrm{d}f, \tag{25}$$

where

$$\tilde{\gamma}(f, d) = \frac{S_0 L(f, d)}{N_0}. \tag{26}$$

From (24) and (25), it is evident that the SNR and achievable capacity depend not only on the transmission distance, the noise PSD and the bandwidth, but also on the reflection surface material as well as the atmospheric conditions.

IV. Results and Discussion

In this section we quantitatively compare the effectiveness of the THz link in terms of SNR and capacity, assuming different transmission bandwidths, central frequencies, as well as atmospheric conditions. For the transmission distance, path lengths ranging from 0.1 to 500 m are considered.

Fig. 2 illustrates the path gain as a function of the frequency for different distances, assuming standard atmospheric conditions, $G_t = G_r = 1$ and $\alpha = \frac{\pi}{3}$. From this figure, it is evident that the path gain decreases as the distance increases with a fixed transmission frequency. For example, for $f = 380$ GHz, as the distance alters from 0.1 to 100 m, the path gain decrease about 100%. This indicates the importance of employing beamforming schemes in order to increase the TX and RX antenna gains and reduce the impact of the channel losses. Additionally, we observe that the frequency dependency, due to the molecular absorption becomes more severe as the distance increases. As a result, the bandwidth of the transparency windows decreases with an increase on the transmission range. For instance, for $d = 0.1$ m, a transparency window exists in the range 275 to 400 GHz with a bandwidth of 125 GHz. On the other hand for $d = 100$ the range of the transparency window is from 330 to 370 GHz and its bandwidth equals 40 GHz, while, for $d = 500$ m, the corresponding window ranges from 340 to 360 GHz. In other words, a five-fold increase in distance results in a 50% decrease of the transparency window.

Fig. 3 demonstrates the detrimental impact of the pathloss due to the distance variation to the received signal quality. We plot the SNR as a function of the distance for different values of $g = G_t G_r S_0 / N_0$ assuming flat transmission signal PSD and $B = 125$ GHz. As expected, for a fixed g, as the distance increases the SNR decreases. For instance, for $g = 120$ dB, a transmission distance increases from 1 to 10 m results in a about 19 dB SNR degradation for both cases of $\alpha = \pi/3$ and without reflections. Moreover, for a given distance, the SNR increases as g increases. For example, for $d = 50$ m, as g increases from 100 to 120 dB, the SNR also increases from -17.5 to 2.4 dB (continious lines) and -16.8 to 3.17 dB (dashed lines). This indicates that in order to increase the link range for a given RX and transmission power, one needs to increase the gain of the TX and/or RX antennas. Finally, this figures reveals the importance of taking into account the impact of reflection on the link budget. For example at $d = 1,\ 50$ and 100 m for all the different values of g, we observe that the combination of the reflected and LOS paths yields almost 1 dB higher SNR compared to only LOS propagation.

In Table I, given at the top of the next page, the capacity is illustrated as a function of the transmission distance for different values of α assuming $g = 120$ dB, $B = 125$ GHz, and standard atmospheric conditions. As expected for a given α, as the distance increases the capacity decreases. Moreover, for a given d as α increases the capacity also increases. In fact, the impact of α becomes more pronounced as d increases. This indicates

TABLE I: The capacity as a function of α and d.

α	$\frac{\pi}{3}$	$\frac{\pi}{4}$	$\frac{\pi}{10}$
$d = 1$ m	1536.12 Gb/s	1536.61 Gb/s	1536.46 Gb/s
$d = 10$ m	698.30 Gb/s	697.86 Gb/s	697.46 Gb/s
$d = 100$ m	61.79 Gb/s	59.27 Gb/s	56.24 Gb/s

the importance of taking into account the reflection angle α, when evaluating the systems performance, especially for longer distances.

V. Conclusions

In this paper, we presented an appropriate channel and system model for THz wireless links in the range of 275 to 400 GHz, which takes into account the channel particularities, the impact of reflections and the transceivers parameters. Moreover, in order to evaluate the effectiveness of the THz system, we evaluated the average SNR and capacity. Our results reveal that the frequency dependency of the THz channel increases, as the range of the wireless link increases. Therefore, in order to achieve acceptable performance in long-range links, high-gain antennas are needed.

Acknowledgment

This work has received funding from the European Commission's Horizon 2020 research and innovation programme under grant agreement No. 761794.

References

[1] A.-A. A. Boulogeorgos and G. K. Karagiannidis, "Low-cost cognitive radios against spectrum scarcity," *IEEE Technical Committee on Cognitive Networks Newsletter*, Nov. 2017.

[2] A.-A. A. Boulogeorgos, "Interference mitigation techniques in modern wireless communication systems," phdthesis, Aristotle University of Thessaloniki, Thessaloniki, Greece, Sep. 2016.

[3] A.-A. A. Boulogeorgos, A. Alexiou, T. Merkle, C. Schubert, R. Elschner, A. Katsiotis, P. Stavrianos, D. Kritharidis, P.-K. Chartsias, J. Kokkoniemi, M. Juntti, J. Lehtomäki, A. Teixeira, and F. Rodrigues, "Terahertz technologies to deliver optical network quality of experience in wireless systems beyond 5G," *IEEE Commun. Mag.*, Jun. 2018.

[4] R. Piesiewicz, T. Kleine-Ostmann, N. Krumbholz, D. Mittleman, M. Koch, J. Schoebei, and T. Kurner, "Short-range ultra-broadband Terahertz communications: Concepts and perspectives," *IEEE Antennas. Propag.*, vol. 49, no. 6, pp. 24–39, Dec 2007.

[5] I. F. Akyildiz, J. M. Jornet, and C. Han, "Terahertz band: Next frontier for wireless communications," *Phys. Commun.*, vol. 12, pp. 16–32, Sep. 2014.

[6] C. Lin and G. Y. L. Li, "Terahertz communications: An array-of-subarrays solution," *IEEE Commun. Mag.*, vol. 54, no. 12, pp. 124–131, Dec. 2016.

[7] A.-A. A. Boulogeorgos, S. Goudos, and A. Alexiou, "Users association in ultra dense thz networks," in *IEEE International Workshop on Signal Processing Advances in Wireless Communications (SPAWC)*, Kalamata, Greece, Jun. 2018.

[8] G. A. Siles, J. M. Riera, and P. G. del Pino, "Atmospheric attenuation in wireless communication systems at millimeter and thz frequencies [wireless corner]," *IEEE Antennas. Propag.*, vol. 57, no. 1, pp. 48–61, Feb. 2015.

[9] A. Afsharinejad, A. Davy, B. Jennings, and C. Brennan, "An initial path-loss model within vegetation in the THz band," in *9th European Conference on Antennas and Propagation (EuCAP)*, May 2015, pp. 1–5.

[10] H. Elayan, R. M. Shubair, J. M. Jornet, and P. Johari, "Terahertz channel model and link budget analysis for intrabody nanoscale communication," *IEEE Trans. Nanobioscience*, vol. 16, no. 6, pp. 491–503, Sep. 2017.

[11] R. Zhang, K. Yang, Q. H. Abbasi, K. A. Qaraqe, and A. Alomainy, "Analytical characterisation of the terahertz in-vivo nano-network in the presence of interference based on TS-OOK communication scheme," *IEEE Access*, vol. 5, pp. 10 172–10 181, 2017.

[12] M. A. Akkas, "Terahertz channel modelling of wireless ultra-compact sensor networks using electromagnetic waves," *IET Commun.*, vol. 10, no. 13, pp. 1665–1672, 2016.

[13] C. Han, A. O. Bicen, and I. F. Akyildiz, "Multi-ray channel modeling and wideband characterization for wireless communications in the terahertz band," *IEEE Trans. Wireless Commun.*, vol. 14, no. 5, pp. 2402–2412, May 2015.

[14] J. M. Jornet and I. F. Akyildiz, "Channel modeling and capacity analysis for electromagnetic nanonetworks in the terahertz band," *IEEE Trans. Wireless Commun.*, vol. 10, no. 10, pp. 3211–3221, Oct. 2011.

[15] P. Boronin, V. Petrov, D. Moltchanov, Y. Koucheryavy, and J. M. Jornet, "Capacity and throughput analysis of nanoscale machine communication through transparency windows in the terahertz band," *Nano Communication Networks*, vol. 5, no. 3, pp. 72–82, 2014.

[16] T. Schneider, A. Wiatrek, S. Preussler, M. Grigat, and R. P. Braun, "Link budget analysis for terahertz fixed wireless links," *IEEE Trans. Terahertz Sci. Technol.*, vol. 2, no. 2, pp. 250–256, Mar. 2012.

[17] A.-A. A. Boulogeorgos, E. N. Papasotiriou, J. Kokkoniemi, J. Lehtomäki, A. Alexiou, and M. Juntti, "Performance evaluation of thz wireless systems operating in 275-400 ghz band," in *IEEE 87th Vehicular Technology Conference: International Workshop on THz Communication Technologies for Systems Beyond 5G*, Porto, Portugal, Jun. 2018.

[18] Z. Xu, X. Dong, and J. Bornemann, "Design of a reconfigurable MIMO system for THz communications based on graphene antennas," *IEEE Trans. Terahertz Sci. Technol.*, vol. 4, no. 5, pp. 609–617, Sep. 2014.

[19] N. Akkari, J. M. Jornet, P. Wang, E. Fadel, L. Elrefaei, M. G. A. Malik, S. Almasri, and I. F. Akyildiz, "Joint physical and link layer error control analysis for nanonetworks in the terahertz band," *Wireless Networks*, vol. 22, no. 4, pp. 1221–1233, May 2016.

[20] J. Lin and M. A. Weitnauser, "Pulse-level beam-switching mac with energy control in picocell terahertz networks," in *IEEE Global Communications Conference (GLOBECOM)*, Austin, TX, USA, Dec. 2014.

[21] J. Kokkoniemi, J. Lehtomäki, and M. Juntti, "Simplified molecular absorption loss model for 275 – 400 gigahertz frequency band," in *Proc. European Conf. Antennas Propag.*, 2018, pp. 1–5.

[22] A.-A. A. Boulogeorgos, E. Papasotiriou, and A. Alexiou, "A distance and bandwidth dependent adaptive modulation scheme for thz communications," in *19th IEEE International Workshop on Signal Processing Advances in Wireless Communications (SPAWC)*, 2018.

[23] O. A. Alduchov and R. E. Eskridge, "Improved magnus form approximation of saturation vapor pressure," *J. Appl. Meteor.*, vol. 35, no. 4, pp. 601–609, Apr. 1996.

[24] A. I. Lvovsky, *Encyclopedia of Optical Engineering*. Taylor and Francis: New York, 2013, ch. Fresnel Equations, pp. 1–6.